ground water

Radar Determination of the Spatial Structure of Hydraulic Conductivity

by Greg A. Oldenborger[1], Robert A. Schincariol[2], and Lalu Mansinha[3]

Abstract/

Spatial variability of hydraulic conductivity exerts a predominant control on the flow of fluid through porous media. Heterogeneities influence advective pathways, hydrodynamic dispersion, and density-dependent dispersion; they are, therefore, a key concern for studies of ground water resource development, contaminant transport, and reservoir engineering. Ground-penetrating radar contributes to the remote, geophysical characterization of the macroscale variability of natural porous media. On a controlled excavation of a glacial-fluvial sand and gravel deposit in the Fanshawe Delta area (Ontario, Canada), the hydraulic conductivity field of a 45 × 3 m vertical exposure was characterized using constant-head permeameter measurements performed on undisturbed horizontal sediment cores. Ground-penetrating radar data were collected along the excavation face in the form of both reflection and common midpoint surveys. Comparison of geostatistical analyses of the permeameter measurements and the radar data suggests that the horizontal correlation structure of radar stack velocity can be used to directly infer the horizontal correlation structure of hydraulic conductivity. The averaging nature of the common midpoint survey is manifest in the vertical correlation structure of stack velocity, making it less useful. Radar reflection data do not exhibit a spatial structure similar to that of hydraulic conductivity possibly because reflections are a result of material property contrasts rather than the material properties themselves.

Introduction

Spatial variability of hydraulic conductivity or intrinsic permeability exerts a predominant control on the flow and transport of fluid in porous media. Order-of-magnitude contrasts in hydraulic conductivity may subtly influence the fluid potential and greatly influence the flow field, thereby producing preferential paths for advective transport (Poeter and Gaylord 1990). Furthermore, heterogeneity of hydraulic properties controls the macrodispersive component of the mechanical dispersion of solutes (Gelhar and Axness 1983; Hess et al. 1992) and, in the case of variable density flow, heterogeneities are a controlling factor in the generation of plume instabilities (Schincariol et al. 1997).

Large-scale descriptions of lithofacies and hydrofacies have proven inadequate for accurate predictions of local ground water flow and contaminant transport and dispersion (Gillham and Cherry 1982; Sudicky et al. 1983; Anderson 1989). Koltermann and Gorelick (1996) reviewed several techniques being developed to address the need for increased spatial resolution of hydraulic property field representations. Generally, these representations may take deterministic or stochastic forms, each of which require prior knowledge of both the probability distribution of the hydraulic property and its spatial correlation structure. To this end, the focus of much recent research has broadened to incorporate geophysical tools into deterministic and stochastic estimations of hydraulic properties (Hyndman and Gorelick 1996; Yamamoto et al. 1995; Cassiani and Medina 1997).

Ground-penetrating radar (GPR) is a near-surface electromagnetic geophysical tool described in detail by Daniels (1996) and Reynolds (1997). Geoscience applications of GPR have traditionally focused on qualitative remote-sensing for determining depths to ground water (Arcone et al. 1998), outlining zones of contamination and sea water intrusion (Davis and Annan 1989) and, most commonly, for imaging the structural architecture of the subsurface

[1]Center for Geophysical Investigation of the Shallow Subsurface, Boise State University, Boise, ID 83725; (208) 426-2716; fax (208) 426-3888; greg@cgiss.boisestate.edu

[2]Department of Earth Sciences, University of Western Ontario, London, Ontario N6A 5B7, Canada; (519) 661-3732; fax (519) 661-3198; schincar@uwo.ca

[3]Department of Earth Sciences, University of Western Ontario, London, Ontario N6A 5B7, Canada; (519) 661-3145; fax (519) 661 3198; lalu@uwo.ca

Received July 2001, accepted July 2002.

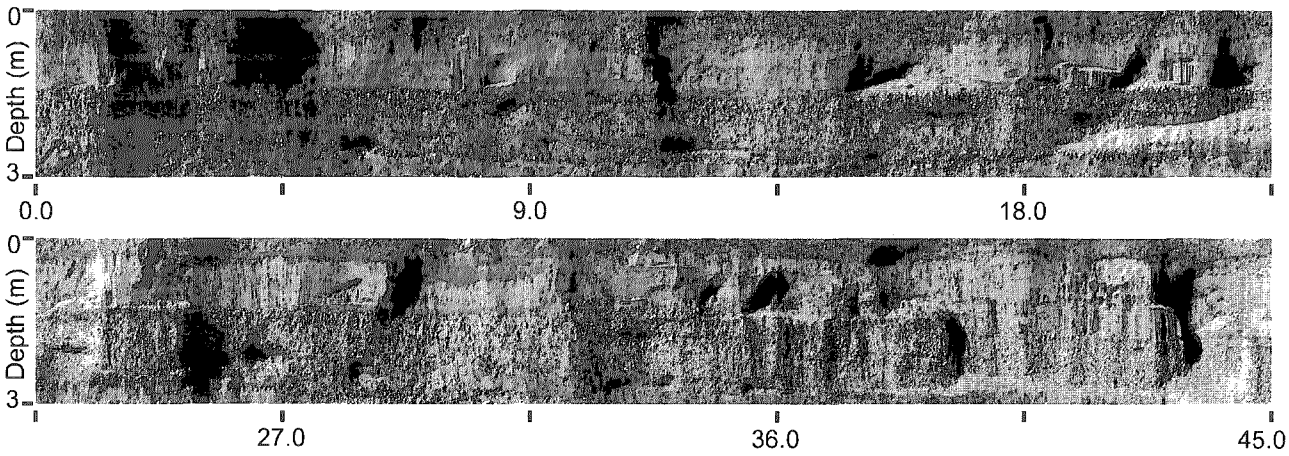

Figure 1. Photographic mosaic of the Fanshawe section. Vertical tick marks delimit 4.5 × 3 m photographic subsections.

(McMechan et al. 1997; Cardimona et al. 1998; Beres et al. 1999). Although structural imaging provides important information on flow conduits and barriers (i.e., hydrofacies distribution), little information is extracted regarding material properties. Most architectural information is not sufficiently quantitative, and the discrimination of heterogeneity is not fine enough to support the stochastic or deterministic generation of hydraulic conductivity fields based on radar reflection data.

Recently, GPR has been incorporated in a more quantitative fashion in attempts to make indirect measurements of hydraulic properties and their spatial correlation structures. In a hydrocarbon context, Baker (1991) illustrated a possible model for relating the radar reflection coefficient to porosity variation. Olhoeft (1994) mapped the continuity of radar reflection patterns to infer the characteristic structural length scales of various sedimentary units. Further, Knight et al. (1996) and Rea and Knight (1998) advanced the working hypothesis that the statistical correlation structure of GPR reflections can be used directly to infer the correlation structure of hydraulic properties. This hypothesis is based on the realization that radar reflections in the subsurface are caused by abrupt changes in the dielectric properties of the geologic materials and that the petrophysical parameters that determine the dielectric properties of a sedimentary unit (grain size, composition, and packing) also determine the hydraulic properties. Several studies have shown either theoretical or experimental relationships between the dielectric properties and the hydraulic conductivity of sedimentary materials (Knoll et al. 1995; Hubbard et al. 1996, 1999a) and Szerbiak et al. (2001) use the statistical structure of radar reflection data to geostatistically continue the permeability field between boreholes in an unsaturated sandstone formation. However, a relationship between the correlation structure of radar reflections and hydraulic conductivity has yet to be demonstrated.

In this work, we concentrate on testing the applicability of surface GPR for the characterization of hydraulic property fields. We have collected sediment cores over a vertical exposure of unsaturated glacial-fluvial sediments and, using GPR, have conducted both reflection and velocity surveys along the top of the exposure. After permeameter analysis of the sediment cores, the relationship between GPR velocity and hydraulic conductivity can be explored. Furthermore, the spatial statistical structure of the radar data can be compared to the spatial statistical structure of the hydraulic conductivity field for this natural, unconsolidated sedimentary deposit.

Study Area

The study area (the Fanshawe section) is in an active gravel pit near London, Ontario, Canada. The site was chosen for its vertical cliff exposure from the active mining of construction materials, for the ease of access, and for its sedimentary nature as an outwash deposit. The Fanshawe Delta is predominantly composed of glacial-fluvial sands and gravels, coarsening from sand and silt in the southwest to alternating beds of sand and gravel in the northeast (Dreimanis et al. 1998). The geological setting combined with observed moderate heterogeneity makes the site applicable as an analogue to a number of other aquifer sediments, such as the Cape Cod Aquifer (Hess et al. 1992).

The Fanshawe section is an approximately north-south striking, vertical exposure of the northern Fanshawe Delta with a horizontal dimension of 45 m and a vertical dimension of 3 m. The deposit consists of horizontally bedded, internally sorted sand and gravel with occasional layers of sandy silt. Some flow features are visible in the section, such as scour depressions and cross beds. The lithology of the gravel is predominantly limestone and dolostone. Cementation is minor and the section is very susceptible to erosion by wind, water, and gravity. The Fanshawe section was surveyed using a Nikon Total Station surveying instrument to define a perimeter grid; a photographic mosaic of the working area is presented as Figure 1. All subsequent sediment core samples and geophysical survey lines were tied into the reference grid.

Hydraulic Data Acquisition

Direct measurements are required to characterize the hydraulic properties of the Fanshawe section deposits as a ground truth for subsequent geophysical surveys; this study concentrates on hydraulic conductivity. The natural hydraulic conductivity field was assessed by performing constant-head permeameter measurements on undisturbed sediment cores (150 mm in length and 73 mm in diameter) obtained using a drive-type Shelby tube sampler (Humboldt

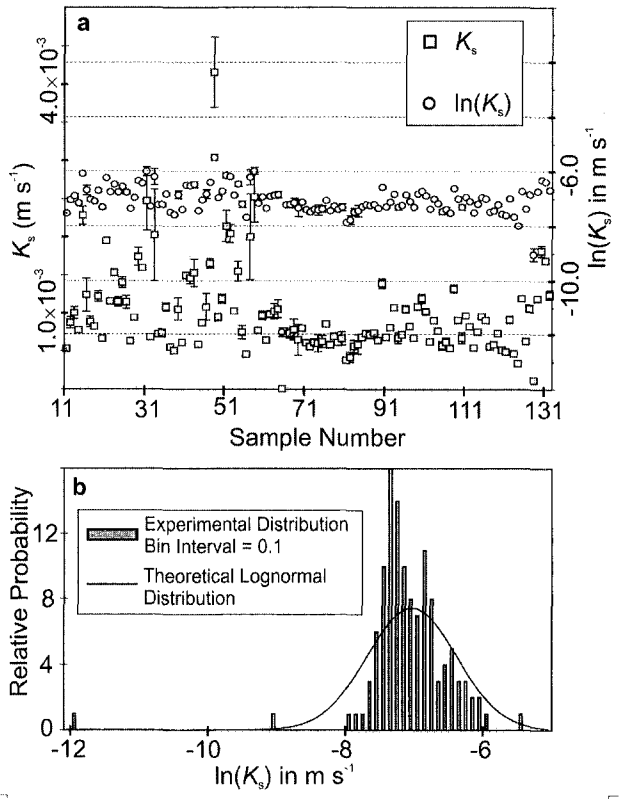

Figure 2. (a) Summary of sample hydraulic conductivities K_s. (b) Frequency distribution for the ln(K_s) data set.

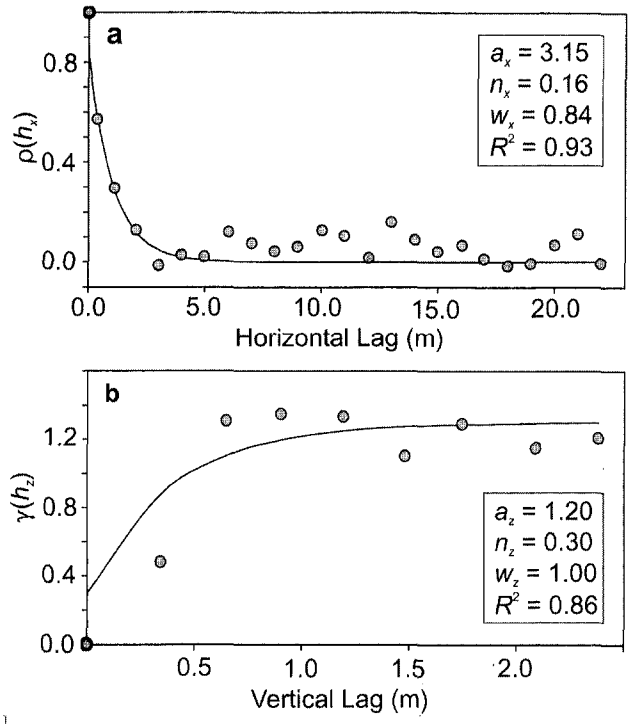

Figure 3. Experimental (points) and model (solid line) geostatistics for the log-transformed hydraulic conductivity data set: (a) horizontal correlogram $\rho(h_x)$; (b) vertical semivariogram $\gamma(h_z)$. Models are fit based on lags up to half the maximum sample separation.

Manufacturing, Raleigh, North Carolina). Sediment cores were oriented horizontally, parallel to bedding structures, such that the core axes were assumed to be aligned parallel to the major axis of the hydraulic conductivity tensor.

In the absence of any prior information regarding the spatial persistence of hydraulic properties at the Fanshawe site, data from the Cape Cod Aquifer (Hess et al. 1992; Eggleston et al. 1996) and the Borden Aquifer (Woodbury and Sudicky 1991) were used to estimate an integral area of 1 m^2 (defined by the correlation lengths of hydraulic conductivity). Eggleston et al. (1996) found that for stochastic simulations of the hydraulic conductivity field, estimation errors reached a minimum asymptote when the sampling density reached a threshold density of approximately three samples per integral volume. Thus, for the Fanshawe section (extending one correlation length in the third dimension) these results provide an estimate of 405 point measurements needed to characterize the exposure. However, logistical constraints and an emphasis on practicality made this number of samples unreasonable. Alternatively, fewer samples can be collected using a random sampling technique for which the threshold sample density can be expected for at least some areas of the Fanshawe section. Therefore, to achieve an average sample density of approximately one sample per estimated integral volume, target locations for 122 sediment cores were established according to a stratified random sampling scheme with uniform block strata (Gilbert 1987). Exact sample locations were surveyed at the field site using a Nikon Total Station. This survey scheme allowed for modification of the sampling strategy of Davis et al. (1997) to address some of the problems that result from constraining samples to a grid such as spatial aliasing and poor detection of subgrid heterogeneity.

Permeameter Analysis

The hydraulic conductivities for the 122 sediment cores were determined using the standard practice of constant-head permeability testing (Cenerica 1995; Burger and Belitz 1997). A summary of the permeameter testing is provided as Figure 2. One-sided error estimates are based on twice the observed standard deviation of four measurements taken at varying flow rates. Total head drops ranged from 0.05 to 0.15 m and fluxes were calculated to be on the order of 10^{-6} m/sec. Samples were removed and examined for any signs of cavitation or segregation of fine material. The majority of the relative errors for the sample hydraulic conductivities K_s are between 0.01 and 0.10. In some cases, however, relative error is in excess of 0.30. In addition to random fluctuations of measurement error from the experimental setup and visual reading of head values, processes such as flow channel development or silt separation may have been active during permeameter experiments even when not observed. Reported errors associated with such samples result primarily from physical changes in the sample over the four separate runs. For example, the possible development of flow channels was noted for sample 57 (Figure 2). Consistent with the development of flow channels, calculated hydraulic conductivities increased with flow rate. Additionally, for samples 64 and 48, silt separation was noted upon removal of the sample from the permeameter and calculated hydraulic conductivities decreased with flow rate consistent with the development of a silt layer at the down-flow porous plate.

Table 1
Summary Statistics of the Hydraulic Conductivity Data Set

	Mean	σ	Maximum	Minimum	Median	df	χ^2	χ^2_c
K_s (m/sec)	9.75×10^{-4}	5.51×10^{-4}	4.16×10^{-3}	6.68×10^{-6}	9.75×10^{-4}	81	111	102
$\ln(K_s)$	−7.08	0.65	−5.48	−11.92	−7.11	63	63	80

Note: σ denotes standard deviation, df indicates degrees of freedom, and χ^2 denotes the chi-squared value.

Table 2
Spatial Descriptors of the Hydraulic Conductivity Data Set

	a_x (m)	Δa_x (m)	w_x	Δw_x	n_x	Δn_x	a_z (m)	Δa_z (m)	w_z	Δw_z	n_z	Δn_z
$\ln(K_s)$ in m/sec	3.15	2.2–4.8	0.84	0.6–1.0	0.16	0.0–0.3	1.20	0.6–1.7	1.00	0.2–1.7	0.30	0.0–0.6

Note: Δ denotes an estimated range of confidence. Other symbols are defined in the text.

Statistical Analysis

The experimental probability distribution for the Fanshawe data set of log-transformed sample hydraulic conductivity $\ln(K_s)$ is illustrated in Figure 3 in comparison to the theoretical normal distribution calculated using the summary statistics of Table 1. Using a chi-square test, the ratios of the calculated chi-square value χ^2 to the critical chi-square value χ^2_c at a 95% significance level are 1.09 and 0.78, respectively, for the K_s and $\ln(K_s)$ distributions. Thus, although the K_s measurements cannot be accepted as normally distributed, $\ln(K_s)$ meets the criterion for a normal distribution. In addition, q-q analysis (Isaaks and Srivastava 1989; Rehfeldt et al. 1992) indicates that $\ln(K_s)$ is the more appropriate choice as the normally distributed variable.

Spatial statistics. Geostatistics is often considered to be the complete set of statistical tools used to both estimate the spatial characteristics/statistics of a sample data set and to make predictions where data are lacking. Of principle concern for estimating spatial persistence is a much smaller subset of geostatistical tools.

Definition of geostatistical estimators is covered extensively by Isaaks and Srivastava (1989) and Deutsch and Journel (1992). The semivariogram for a random variable $g(\mathbf{r}_i)$ is calculated as half of the average squared difference between variable values separated by a lag vector $\mathbf{h}$:

$$\gamma(\mathbf{h}) = \frac{1}{2\sigma^2 N(\mathbf{h})} \sum_{i=1}^{N} \left(g(\mathbf{r}_i) - g(\mathbf{r}_i - \mathbf{h}) \right)^2 \qquad (1)$$

where $\mathbf{r}_i$ is the position vector of the ith measurement, N is the number of measurements separated by $\mathbf{h}$, and σ^2 is the sample set variance. The semivariogram can be understood as the normalized sample variance described as a function of spatial separation. Thus, low semivariogram values indicate a high degree of correlation between variable values separated by the lag vector.

The correlogram, or correlation function

$$\rho(\mathbf{h}) = \frac{1}{\sigma_{-h}\,\sigma_{+h}\,N(\mathbf{h})} \sum_{i=1}^{N} g(\mathbf{r}_i)\, g(\mathbf{r}_i - \mathbf{h}) - \bar{g}_{-h}\,\bar{g}_{+h} \qquad (2)$$

also describes the sample set variance as a function of the lag vector where $\sigma_{\pm h}$ and $g_{\pm h}$ are the head and tail standard deviations and means, respectively. Theoretically, $\gamma(\mathbf{h}) = 1 - \rho(\mathbf{h})$, but explicit incorporation of the head and tail standard deviations and means into the calculation of the discrete correlogram renders it more resistant to data sparsity, outliers, clustering, and sampling error (Deutsch and Journel 1992).

In this work, the more familiar semivariogram is used as the primary estimator of spatial persistence; in most cases, it is sufficient to reveal the nature of the variability. However, the horizontal semivariogram of hydraulic conductivity does not render an easily recognizable geostatistical trend. In this case, the more robust correlogram is used as the measure of variability. All experimental geostatistics were calculated using the popular GSLIB routines (Deutsch and Journel 1992).

Experimental semivariograms are fit using exponential models of the form

$$\gamma(h) = n + \sum_i w_i \left(1 - \exp\{-3h/a_i\}\right) \qquad (3)$$

where h is the lag vector magnitude in a specified direction, w is the weight, n is the nugget effect, and a is the practical range; several exponential models may be combined or nested.

Experimental and model geostatistics are shown for the $\ln(K_s)$ data in Figure 3. Model parameters are fit to the experimental geostatistics based on minimization of the sum of the squares of the residuals between the experimental and model statistics; the residuals at zero lag are not incorporated in any solutions. Spatial descriptors of the

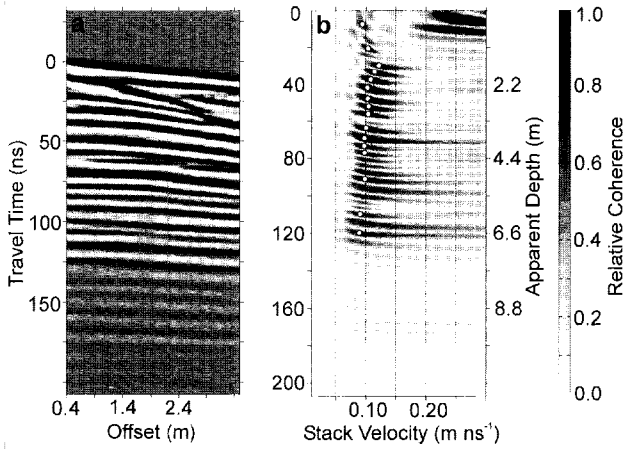

Figure 4. (a) CMP radar gather centered at 25 m along the Fanshawe section. The direct ground wave allows for estimation of the surface propagation velocity V_{ground} = 0.10 m/ns which is typical for sand or gravel deposits with low moisture content. (b) NMO stack velocity spectrum for the CMP gather centered at 25 m. Open circles indicate picked points of maximum coherence that define the velocity profile.

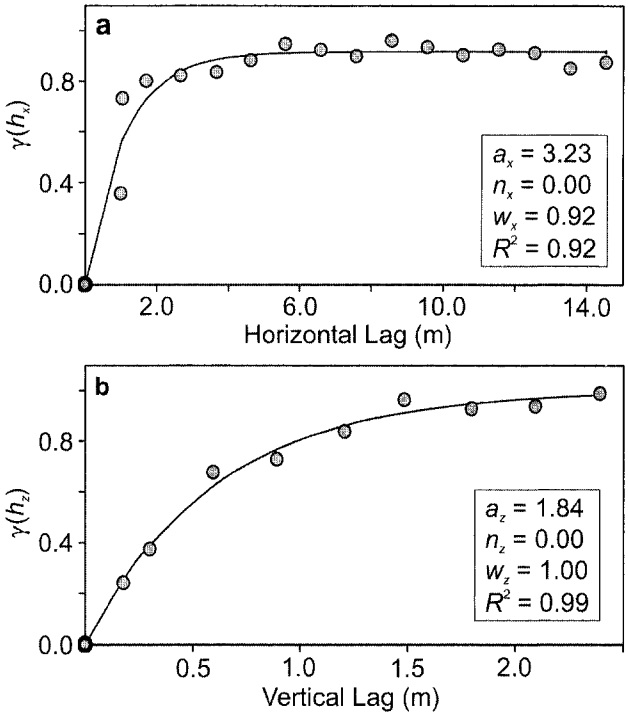

Figure 5. Experimental (points) and model (solid line) geostatistics for the stack velocity data set: (a) horizontal semivariogram $\gamma(h_x)$; (b) vertical semivariogram $\gamma(h_z)$. Models are fit based on lags up to half the maximum sample separation.

data are summarized in Table 2. Confidence ranges for the estimated spatial parameters of the hydraulic conductivity data are obtained based on the envelope provided by the theoretical precision of the statistical estimator, which is a function of the number of sample pairs at each lag (Rehfeldt et al. 1992; Zheng and Silliman 2000).

In light of the geostatistical parameters, the integral area of the Fanshawe section can be calculated to be 0.47 m^2. Approximately one sample was taken for every two integral areas. It is evident from the experimental semivariograms that variogram modelling suffers from data sparsity in the vertical direction. Because the vertical range is much smaller than the horizontal range, a greater number of sample pairs at smaller separations are required for more confident estimation of the vertical correlation structure.

Ground-Penetrating Radar

Data Acquisition

All radar data were collected with a Pulse Ekko 100 bistatic radar system with a central antenna frequency of 200 MHz, a 400 V transmitter, and 64-trace stacking. Initial experiments with 100 MHz antennae showed increased depth of penetration (~10 m). The 200 MHz setup was employed to take advantage of an increase in resolution with frequency (Annan and Davis 1977). Located with respect to the perimeter grid, a primary GPR survey line was defined parallel to the cliff face of the Fanshawe section from 0.0 to 50.0 m. Reflection data were collected along the survey line with station spacings of 0.1 m and an antenna separation of 0.5 m. Common midpoint (CMP) gathers were collected at 1 m intervals with a 0.1 m offset step-size and 32 traces per gather. All radar signals were sampled in time using an 800 ps sample interval.

Velocity Analysis

A principal assumption of most GPR surveys is that the subsurface can be considered to be a nonmagnetic insulator or a low-loss environment such that conductive currents and, thus, conductive energy losses are minimal. Typically, the low-loss assumption can be accepted for propagation frequencies between 100 MHz and 1 GHz, provided that the electrical conductivity of the medium is < 100 mS/m (Davis and Annan 1989). The velocity of an electromagnetic wave in a low-loss environment (neglecting frequency dependence) is given by

$$V = \frac{c}{\sqrt{\varepsilon_r \mu_r}} \tag{4}$$

where c is the speed of light in a vacuum, ε_r is the relative dielectric constant, and $\mu_r = 1$ is the relative magnetic permeability.

For surface determination of radar wave velocity, the CMP survey and normal-moveout (NMO) velocity analysis are applicable to GPR data (Fisher et al. 1992; Greaves et al. 1996). For the Fanshawe section, CMP preprocessing required subtraction of the exponential baseline (often referred to as wow) associated with low frequency induction effects (and possibly saturation of instrument electronics). The only other preprocessing step was the application of an adaptive automatic gain control (AGC) time-gain function to compensate for the decaying amplitude of the radar signal with travel-time. For example, the gained CMP gathered at 25 m is presented as Figure 4a.

To determine information regarding the variation of radar velocity with depth, a velocity spectrum is constructed for each CMP gather. Following the algorithm outlined by Yilmaz (1987), the small-dip, small-offset approximation was used to generate stacked coherence maps as

Table 3
Statistics of the Stack Velocity Data Set

	Mean	σ	a_x (m)	w_x	n_x	a_z (m)	w_z	n_z
V_s (m/ns)	0.110	0.009	3.23	0.92	0.00	1.84	1.00	0.00

Note: See text for symbol definition.

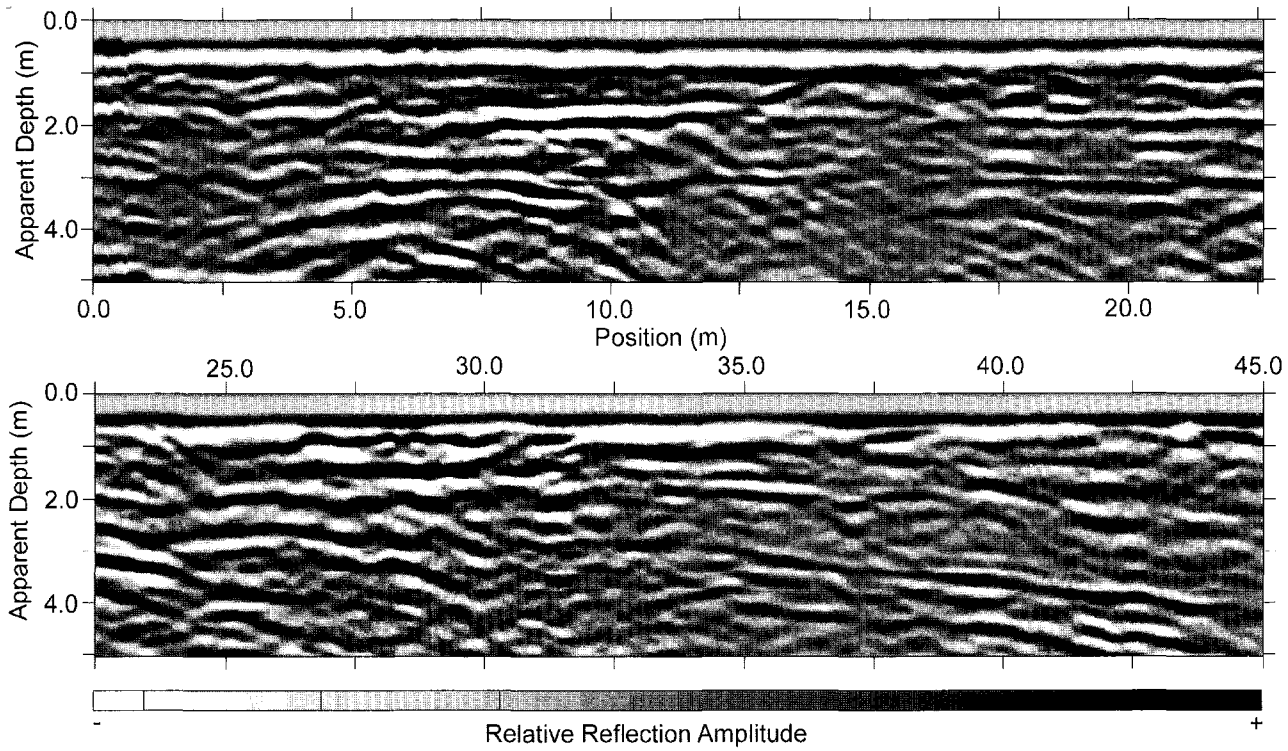

Figure 6. Radar reflection profile along the Fanshawe section with 200 MHz antenna frequency.

functions of zero-offset travel-time and stack velocity V_s. The coherence map for the CMP data centered at 25 m is displayed in Figure 4b as an example.

Points of maximum coherence were hand-picked according to well-defined coherence maxima with minimal smearing (Fig. 4). Smearing of the coherence plot is a combined result of noise, intermittent reflectors and violation of the small-offset assumption at late times. All early-time high coherence zones contaminated by air arrivals ($V_s > 0.2$ m/ns) are ignored and lower coherency zones within the 0 to 25 ns time window that are masked by air arrivals are picked according to relative coherence at early times. The result is a series of stack velocity profiles as functions of travel-time at 1 m intervals along the Fanshawe section.

Stack velocity, however, is not the most geologically meaningful quantity insofar as it involves the averaging of the radar velocity along the raypath; for horizontally stratified materials, the stack velocity is an approximate root-mean-square (RMS) velocity. To remove the RMS effect, the Dix inversion was applied while taking care to account for decreasing radar velocity with depth (Greaves et al. 1996).

Spatial statistics. Given the radar wave velocity as a function of position and travel-time, the geostatistics of the velocity field can be calculated, provided that travel-time can be translated to depth. The mean stack velocity is 0.110 m/ns with a standard deviation of 0.009 m/ns. The low standard deviation of stack velocity allows use of a constant velocity of 0.11 m/ns for approximate depth conversions.

The experimental semivariograms of Dix velocity are very erratic and exhibit length scales below the minium data separation, which prohibits reliable modeling. This is a manifestation of the known instability of the Dix inversion as reported by Greaves et al. (1996), who find it necessary to employ a smoothing filter to calculated Dix velocities, thereby artificially increasing the spatial continuity.

The geostatistical models of stack velocity, however, are simple exponentials with good low-lag definition (Figure 5). It is observed that the modeled horizontal range for the stack velocity field is very similar to the horizontal range for the hydraulic conductivity field (Table 3). The modeled vertical range of stack velocity is somewhat larger than that of hydraulic conductivity (Tables 2 and 3); this increased vertical range represents the vertical averaging inherent to the CMP method of velocity determination. Unless there is a rapid change of sedimentary structure in the horizontal direction, it can be assumed that the averaged nature of stack velocity is limited to the vertical direction and that the horizontal correlation structure of stack

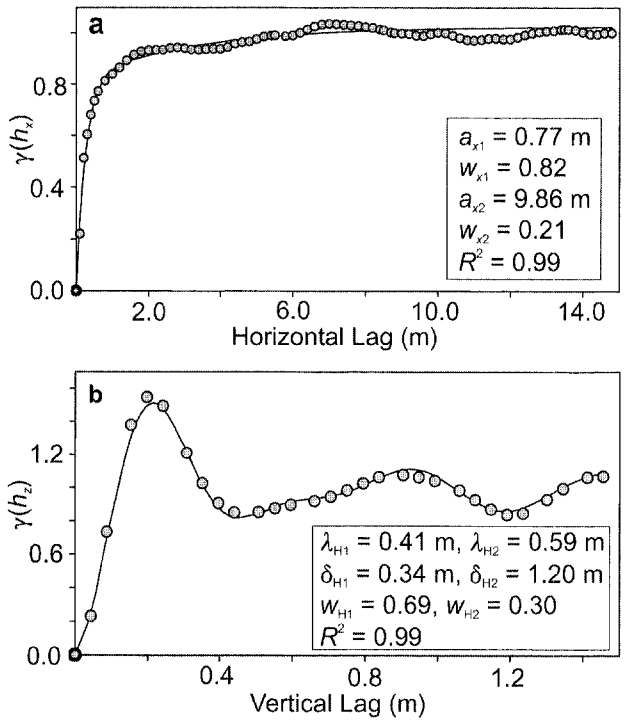

Figure 7. Experimental (points) and model (solid line) geostatistics for the radar reflection amplitude data set: (a) horizontal semivariogram $\gamma(h_x)$; (b) vertical semivariogram $\gamma(h_z)$.

velocity is, in fact, representative of the correlation structure of hydraulic conductivity.

Allowing for horizontal and vertical tolerances of ± 0.25 m (based on approximate radar resolution), 19 measurements of hydraulic conductivity are collocated with measurements of stack velocity. Correlation between the two variables, however, is less than statistically significant. The lack of correlation is caused, at least in part, by the vertical averaging present in the CMP data. More success at developing functional relationships between radar wave velocity and material properties has been shown for vertical radar profiling (Knoll and Clement 1999) and borehole travel-time tomography (Hubbard et al. 1999b) for which ray-path averaging is accounted for and for which the number of collocated data pairs is much larger.

Reflection Analysis

The initial preprocessing steps for the reflection data were equalization in time of the first breaks, removal of any zero-frequency bias, and subtraction of the exponential baseline. The only additional processing prior to geostatistical analysis was to apply a time-gain function to correct for amplitude decay because of attenuation and geometrical spreading of the radar signal. To retain amplitude relationships both down-trace and between traces, a spreading exponential compensation (SEC) time-gain function was applied to the reflection data for the Fanshawe section. Alternative gain functions (such as AGC) that attempt to equalize signal amplitudes destroy relative amplitude relations and contribute to artificially increased continuity of the reflection data. The gained radar reflection profile along the Fanshawe section is presented as Figure 6 with apparent depth estimated using the average velocity of 0.11 m/ns.

Spatial statistics. The high sample density of the radar reflection data makes for strong estimates of the semivariogram measure of spatial persistence. However, to avoid incorporating the exceptionally coherent early time air and direct ground waves (and to avoid data in violation of the zero-offset assumption), data recorded before 20 ns (1.1 m apparent depth) are not used in the geostatistical calculations. Similarly, although reflection data are reliable to 150 ns (8.25 m apparent depth), only the data above 75 ns (4.1 m apparent depth) are considered such that the area of analyzed reflections equals that of the sediment core data and does not extend too far below the exposed Fanshawe section.

Figure 7 shows the experimental and model geostatistics for radar reflection amplitude. It is evident that the low-lag definition of the semivariogram is high, which leads to zero nugget effect in both the vertical and horizontal directions. In the horizontal direction, it is necessary to employ a nested semivariogram model to capture the initial sharp rise in the variance followed by a slower approach to the asymptote. The nested model indicates the presence of features with two different exponential length scales of a_{x1} = 0.77 m and a_{x2} = 9.86 m. If the data are fit with a simple exponential model, the optimum length scale is ~1.5 m, but neither the low- nor high-lag data are fit well.

In the vertical direction, the experimental semivariogram exhibits an oscillatory hole effect, which is often observed for data sets characterized by a natural periodicity. The hole effect can be modeled by

$$\gamma(h) = w_H \left(1 - \exp\left\{-\frac{h}{\delta_h}\right\} \cos\left(\frac{2\pi h}{\lambda_H}\right)\right) \qquad (5)$$

where w_H is the weight, λ_H is the hole wavelength, and δ_H is the damping factor. The optimum model for the vertical semivariogram is a double hole effect with wavelengths of 0.41 and 0.59 m. These wavelengths are too small to be attributed to periodicity of the observed sedimentary units (Oldenborger et al. 2002). However, both wavelengths are similar in scale to the wavelet nature of the incident radar pulse (Rea and Knight 1998). The need for nested hole models may be indicative of frequency dispersion of the radar signal.

The correlation structure and characteristic length scales determined for the radar reflection profile are markedly different from those determined for the hydraulic conductivity and the stack velocity data sets. In the horizontal direction, two length scales are active. Although scale-dependence of hydraulic properties is a recognized phenomenon, variability between within-facies and combined-facies spatial persistence in the horizontal direction is expected to be negligible (Davis et al. 1997). The longer horizontal range is suspected to be representative of the persistence of the boundaries between sedimentary units, whereas the ranges of the hydraulic conductivity and the stack velocity data sets represent persistence of material properties. The shorter horizontal range is suspected to be representative of the smaller scale discontinuities in reflection amplitude that are attributable to scattering, random noise, and static elevation errors. Similarly, Rea and Knight

(1998) note that dipping reflectors will contribute to short-range characteristic length scales because they will cut across the lag vector and that, for GPR survey areas with steeply dipping reflectors, migration might be a necessary additional processing step for accurately locating reflectors in space. However, application of a constant-velocity f-k migration routine was found to have no effect on the geostatistical analysis of the Fanshawe reflection data sets.

Additionally, we recognize that the horizontal and vertical directions may not be the directions of maximum and minimum correlation. However, when comparing the spatial structure of different data, it is consistency of direction that is important.

Conclusions

Presently, the advancement of the practice of predicting ground water flow and the fate of contaminant transport is limited to a large extent by the inability to efficiently characterize the subsurface heterogeneity of porous media. For the Fanshawe section, drive-type sampling proved successful in the acquisition of undisturbed sediment cores and constant-head permeameter testing of the cores provided relatively low-error characterization of the actual hydraulic conductivity field in terms of a probability distribution and geostatistical characteristics. A stratified random sampling scheme with a sample density of approximately one sample for every two integral areas was effective at providing sufficient data pairs for a confident estimation of the horizontal spatial correlation structure of hydraulic conductivity. Despite the random sampling scheme, the sampling campaign suffered from a sparsity of samples separated by vertical distances less than the vertical range of the hydraulic conductivity field. Unfortunately, the destructive nature of sampling the unconsolidated cliff face precluded a second sampling campaign. When obtaining sediment cores for point measurements of hydraulic conductivity, it would be advantageous to include a small-scale, high-density sampling campaign—at least over several integral areas—in addition to a low-density, regional stratified random sampling scheme.

Surface CMP and reflection GPR surveys were conducted along the Fanshawe section. Velocity analysis of the CMP surveys allowed for the construction of a stack velocity data set over the section. Despite vertical averaging associated with CMP velocity determination, the correlation structure of stack velocity is similar to that of hydraulic conductivity and the horizontal range of stack velocity can be used to directly infer the horizontal range of log-transformed hydraulic conductivity. Accordingly, surface velocity determination may prove useful in characterizing the spatial distribution of hydraulic properties. For example, well-logging provides material measurements that are vertically dense but horizontally sparse. Dense vertical information can be used to estimate the mean, variance, and vertical range of hydraulic properties and CMP surveys may be used to estimate the horizontal correlation structure: a necessity for the deterministic or stochastic estimation of the continuous hydraulic property field.

The more commonly encountered reflection surveys provided little information about spatial correlation structure of hydraulic conductivity. Geostatistical analyses of reflection data appear to yield information on the correlation structure of sedimentary boundaries; the spatial persistence of radar reflection amplitude was not observed to be similar to the spatial persistence of the hydraulic conductivity as measured for the sediment cores. This observation is most readily explained by the fact that radar reflection amplitude is proportional to the contrast or discontinuity in dielectric properties. Thus, rather than mapping material properties, a GPR reflection profile is more a map of the spatial rate of change of material properties. This derivative-like nature of GPR reflectivity is manifest in the increased horizontal range of the reflection profiles in comparison to those of the velocity and hydraulic conductivity data sets. Given the physical nature of radar reflections, questions remain as to the cause of subfacies radar reflections and their significance.

Acknowlegments

This research was funded by the Natural Sciences and Engineering Research Council of Canada through grants awarded to authors RAS and LM and a postgraduate scholarship awarded to GAO. Lafarge Canada Inc. kindly provided access to their London gravel pits and the loan of heavy machinery. The authors would like to thank J.D. McNeil for assistance with field data acquisition, M.D. Campbell, T. Griffin, and an anonymous reviewer for constructive comments and criticisms and M.D. Knoll for helpful discussions.

Editor's Note: The use of brand names in peer-reviewed papers is for identification purposes only and does not constitute endorsement by the authors, their employers, or the National Ground Water Association.

References

Anderson, M.P. 1989. Hydrogeological facies models to delineate large-scale spatial trends in glacial and glaciofluvial sediments. *Geological Society of America Bulletin* 101, 501–511.

Annan, A.P., and J.L. Davis. 1977. Radar range analysis for geological materials. *Geological Survey of Canada, Report of Activities* 77-1B, 117–124.

Arcone, S.A., D.E. Lawson, A.J. Delaney, J.C. Strasser, and J.D. Strasser. 1998. Ground-penetrating radar reflection profiling of groundwater and bedrock in an area of continuous permafrost. *Geophysics* 63, no. 5: 1573–1584.

Baker, P.L. 1991. Fluid, lithology, geometry, and permeability information from ground-penetrating radar for some petroleum industry applications. *Society of Petroleum Engineers*, SPE 22976: 277–287.

Beres, M., P. Huggenberger, A.G. Green, and H. Horstmeyer. 1999. Using two- and three-dimensional georadar methods to characterize glaciofluvial architecture. *Sedimentary Geology* 129, nos. 1-2: 1–24.

Burger, R.L., and K. Belitz. 1997. Measurement of anisotropic hydraulic conductivity in unconsolidated sands: A case study from a shoreface deposit, Oyster, Virginia. *Water Resources Resources* 33, no. 6: 1515–1522.

Cardimona, S.J., W.P. Clement, and K. Kadinsky-Cade. 1998. Seismic reflection and ground-penetrating radar imaging of a shallow aquifer. *Geophysics* 63, no. 4: 1310–1317.

Cassiani, G., and M.A. Medina Jr. 1997. Incorporating auxiliary geophysical data into ground-water flow parameter estimation. *Ground Water* 35, no. 1: 79–91.

Cenerica, J.N. 1995. *Geotechnical Engineering: Soil Mechanics*. New York: John Wiley and Sons.

Daniels, D.J. 1996. *Surface-Penetrating Radar*. London: Institution of Electrical Engineers.

Davis, J.L., and A.P. Annan. 1989. Ground-penetrating radar for high resolution mapping of soil and stratigraphy. *Geophysical Prospecting*. 37, 531–551.

Davis, J.M., J.L. Wilson, F.M. Phillips, and M.D. Gotkowitz. 1997. Relationship between fluvial bounding surfaces and the permeability correlation structure. *Water Resources Research* 33, no. 8: 1843–1854.

Deutsch, C.V., and A.G. Journel. 1992. *GSLIB: Geostatistical Software Library and User's Guide*. New York: Oxford University Press.

Dreimanis, A., C.G. Winder, and R.A. Aaltonen. 1998. London, Ontario: Geology, geomorphology, geodata. In *Urban Geology of Canadian Cities*, ed. P.F. Karrow and O.L. White, 237–260. St. John's, Newfoundland, Canada: Geological Association of Canada.

Eggleston, J.R., S.A. Rojstaczer, and J.J. Peirce. 1996. Identification of hydraulic conductivity structure in sand and gravel aquifers: Cape Cod data set. *Water Resources Research* 32, no. 5: 1209–1222.

Fisher, E., G.A. McMechan, and A.P. Annan. 1992. Acquisition and processing of wide-aperture ground-penetrating radar. *Geophysics* 57, no. 3: 495–504.

Gelhar, L.W., and C.L. Axness. 1983. Three-dimensional stochastic analysis of macrodispersion in aquifers. *Water Resources Research* 19, no. 1: 161–180.

Gilbert, R.O. 1987. *Statistical Methods for Environmental Pollution Monitoring*. New York: Van Nostrand Reinhold.

Gillham, R.W., and J.A. Cherry. 1982. Contaminant migration in saturated unconsolidated geologic deposits. *Geological Society of America Special Paper* 189, 31–62.

Greaves, R.J., D.P. Lesmes, J.M. Lee, and M.N. Toksöz. 1996. Velocity variations and water content estimated from multi-offset, ground-penetrating radar. *Geophysics* 61, no. 3: 683–695.

Hess, K.M., S.H. Wolf, and M.A. Celia. 1992. Large scale natural gradient tracer test in sand and gravel, Cape Cod, Massachusetts: 3. Hydraulic conductivity variability and calculated macrodispersivities. *Water Resources Research* 28, no. 8: 2011–2027.

Hubbard, S.S., E. Majer, J. Geller, J. Peterson, and B. Parsons. 1996. Permeability estimation using geophysical data. *EOS Transactions* 77, no. 46: F220.

Hubbard, S.S., J. Chen, Y. Rubin, E. Major, and J.E. Peterson Jr. 1999a. Log-permeability estimation using multiple geophysical data sets in a Bayesian framework. *EOS Transactions* 80, no. 17: S120.

Hubbard, S.S., Y. Rubin, and E. Majer. 1999b. Spatial correlation structure estimation using geophysical and hydrogeological data. *Water Resources Research* 35, no. 6: 1809–1825.

Hyndman, D.W., and S.M. Gorelick. 1996. Estimating lithologic and transport properties in three dimensions using seismic and tracer data: The Kesterson aquifer. *Water Resources Research* 32, no. 9: 2659–2670.

Isaaks, E.H., and R.M. Srivastava. 1989. *An Introduction to Applied Geostatistics*. New York: Oxford University Press.

Knight, R., J. Rea, and P. Tercier. 1996. Geostatistical analysis of ground penetrating radar data: A means of characterizing the correlation structure of sedimentary units. *EOS Transactions* 77, no. 46: F237.

Knoll, M.D., R. Knight, and E. Brown. 1995. Can accurate estimates of permeability be obtained from measurements of dielectric properties? *Proceedings of the Symposium on the Application of Geophysics to Engineering and Environmental Problems*, 25–35. Denver, Colorado: Environmental and Engineering Geophysical Society.

Knoll, M.D., and W.P. Clement. 1999. Vertical radar profiling to determine dielectric constant, water content and porosity values at well locations. *Proceedings of the Symposium on the Application of Geophysics to Engineering and Environmental Problems*, 821–830. Denver, Colorado: Environmental and Engineering Geophysical Society.

Koltermann, C.E., and S.M. Gorelick. 1996. Heterogeneity in sedimentary deposits: A review of structure-imitating, process-imitating and descriptive approaches. *Water Resources Research* 32, no. 9: 2617–2658.

McMechan, G.A., G.C. Gaynor, and R.B. Szerbiak. 1997. Use of ground-penetrating radar for 3-D sedimentological characterization of clastic reservoir analogs. *Geophysics* 62, no. 3: 786–796.

Oldenborger, G.A., R.A. Schincariol, and L. Mansinha. 2002. Space-local spectral texture segmentation applied to characterizing the heterogeneity of hydraulic conductivity. *Water Resources Research* 38, no. 8: 10.1029/2001 WR00026 2002.

Olhoeft, G.R. 1994. Quantitative statistical description of subsurface heterogeneities with ground penetrating radar at Bemidji, Minnesota. U.S. Geological Survey Water Investigation Report 91-4034: 650–653.

Poeter, E., and D.R. Gaylord. 1990. Influence of aquifer heterogeneity on contaminant transport at the Hanford site. *Ground Water* 28, no. 6: 900–909.

Rea, J., and R. Knight. 1998. Geostatistical analysis of ground-penetrating radar data: A means of describing spatial variation in the subsurface. *Water Resources Research* 34, no. 3: 329–339.

Rehfeldt, K.R., J.M. Boggs, and L.W. Gelhar. 1992. Field study of dispersion in a heterogeneous aquifer: 3. Geostatistical analysis of hydraulic conductivity. *Water Resources Research* 28, no. 8: 3309–3324.

Reynolds, J.M. 1997. *An Introduction to Applied and Environmental Geophysics*. Chichester, United Kingdom: John Wiley and Sons.

Schincariol, R.A., F.W. Schwartz, and C.A. Mendoza. 1997. Instabilities in variable density flows: Stability and sensitivity analysis for homogeneous and heterogeneous media. *Water Resources Research* 33, no. 1: 31–41.

Sudicky, E.A., J.A. Cherry, and E.O. Frind. 1983. Migration of contaminants in groundwater at a landfill: A case study. *Journal of Hydrology* 63, 81–108.

Szerbiak, R.B., G.A. McMechan, R. Corbeanu, C. Forster, and S.H. Snelgrove. 2001. 3-D characterization of a clastic reservoir analog: From 3-D GPR data to a 3-D fluid permeability model. *Geophysics* 66, no. 4: 1026–1037.

Woodbury, A.D., and E.A. Sudicky. 1991. The geostatistical characteristics of the Borden aquifer. *Water Resources Research* 27, no. 4: 533–546.

Yamamoto, T., T. Nye, and M. Kuru. 1995. Imaging the permeability structure of a limestone aquifer by crosswell acoustic tomography. *Geophysics* 60, no. 6: 1634–1645.

Yilmaz, Ö. 1987. *Seismic Data Processing: Investigations in Geophysics, No. 2*. Tulsa, Oklahoma: Society of Exploration Geophysicists.

Zheng, L., and S. E. Silliman. 2000. Estimating the theoretical semivariogram from finite numbers of measurements. *Water Resources Research* 36, no. 1: 361–366.